SIMULATION OF CHARGED PARTICLE TRANSPORT ON THE MPP

James A. Earl
University of Maryland
Department of Physics and Astronomy
College Park, MD 20742

ABSTRACT

Computations of cosmic-ray transport based upon finite-difference methods are afflicted by instabilities, inaccuracies, and artifacts. To avoid these problems, we have developed a Monte Carlo formulation which is closely related not only to the finite-difference formulation, but also to the underlying physics of transport phenomena. Implementations of this approach are currently running on the Massively Parallel Processor at Goddard Space Flight Center, whose enormous computing power overwhelms the poor statistical accuracy that usually limits the use of stochastic methods. In a Monte Carlo simulation of rectilinear transport, the coherent and diffusive effects that appeared are in good quantitative agreement with both finite-difference and analytic calculations.

Keywords: cosmic-rays, interplanetary medium, magnetic fields, particle transport

INTRODUCTION

The diffusion idealization, which has been almost universally invoked in discussions of cosmic-ray transport, is easy to treat analytically. However, many observed phenomena give clear evidence for non-diffusive effects. One example is the so-called "scatter free" propagation of kilovolt solar electrons (Ref. 1), which is inconsistent with diffusion, but which can readily be interpreted in terms of a coherent mode of propagation. This mode is novel, but it is just a manifestation in a dynamic situation of non-diffusive effects similar to those considered in the steady-state by classical transport theory (Ref. 2). Although these effects have been described analytically in References 3 and 4, the theory is very complicated. Consequently, there is a need for reliable numerical computations which bypass these complexities and yield concrete results suitable for comparison with observations. This paper explores such computations based on the well-known Monte Carlo method and compares them to computations based upon finite-difference methods. To limit the number of parameters, and to focus the discussion on computational methods, the present discussion is limited to the case of rectilinear one-dimensional propagation of cosmic-rays along a uniform magnetic guiding field on which are superimposed random fields. This leaves out the effects of adiabatic focusing by non uniform guiding fields and of convective motion of the background medium, which are very important in the interplanetary context, but it includes two other essential aspects of charged particle transport. These are a strong inhibition of transport perpendicular to the guiding field and a pronounced anisotropy of the pitch-angle scattering by random fields. Finally, note that the magnetic fields are visualized as static, which means that the velocities of individual particles are constant, and that there is no interaction among particles in the extremely tenuous distribution of cosmic-rays. This situation differs from those considered by plasma physics, but it is closely analogous to those treated by classical transport theory.

TRANSPORT EQUATIONS

Under the circumstances outlined above, particle transport is described by

$$\frac{\partial f}{\partial s} + \mu\frac{\partial f}{\partial z} = \frac{\partial}{\partial \mu}\,\psi\,\frac{\partial f}{\partial \mu}, \qquad (1)$$

in which f is particle density in phase space, μ is the cosine of the pitch-angle measured with respect to the guiding field, and z is distance parallel to the guiding field. The variable $s = Vt$, where V is particle velocity, plays the role of a temporal parameter. The Fokker-Planck coefficient of pitch-angle scattering is given by

$$\psi = \frac{(3/2\lambda)}{(2-q)(4-q)}\,(1-\mu^2)\,|\mu|^{q-1}, \qquad (2)$$

where λ is the mean free path, and q is an index that measures the anisotropy of scattering (Ref. 5).

In the discrete formulation, the continuous variables are replaced by a three-dimensional grid whose spacings are Δz, $\Delta\mu$, and $\Delta s = V\Delta t$, and the derivatives appearing in equation (1) are replaced by their finite-difference analogs. These replacements lead to the difference equation

$$\begin{aligned}\Delta f = {} & P_{M+\frac{1}{2}}(f_{M+1,Z} - f_{M,Z}) \\ & + p_{m-\frac{1}{2}}(f_{M,Z} - f_{M-1,Z}) \\ & + \mu_M(_{M,Z-1} - f_{M,Z}),\end{aligned} \qquad (3)$$

which gives the change in the distribution function during a temporal increment Δs, and which can readily be solved by standard numerical methods. In the Monte Carlo formulation, the random history of a large number of particles is followed under the assumption that the coefficients $P_{M\pm1/2}$ appearing in equation (3) can be interpreted as probabilities that μ will change by $\pm\Delta\mu$ in each time step. In this formulation, the particles move a distance $\mu\,\Delta S$ in each step. This slight difference in the evolution of z from that described by the finite-difference formulation, has a significant effect that will be discussed below.

In Figure 1, the transition probabilities are plotted as a function of μ for two different assumptions about the anisotropy of scattering. Both curves refer to the same mean free path, $\lambda = 480$. The square symbols describe strongly anisotropic scattering ($q = 1.8$) similar to that occurring in interplanetary space. Evidently, the scattering near $\mu = 0$, which is the boundary between forward ($\mu > 0$) and backward ($\mu < 0$) hemispheres, is much weaker than that occurring within each hemisphere. Consequently, this boundary acts as a physically significant barrier which particles find difficult to penetrate. In contrast, the circular symbols, which refer to isotropic scattering ($q = 1.0$) similar to that occurring in molecular collisions or neutron diffusion, describe relatively weak and nearly uniform scattering with no feature at $\mu = 0$.

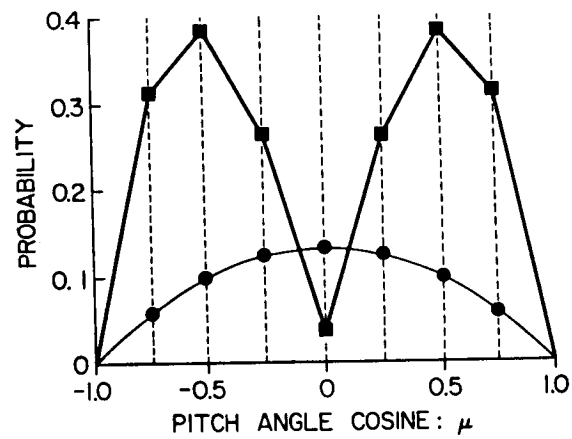

Figure 1. Scattering probabilities for $\lambda = 480$ plotted as a function of pitch-angle cosine. The square points for anisotropic scattering define a curve that is qualitatively different from the one defined for classical isotropic scattering by circular points.

THE ALGORITHM

To implement the Monte Carlo scheme outlined above, each particle was assigned an integer distance and an index corresponding to μ that lies between 0 and 7. Because these parameters occupy only three bytes, there was plenty of storage for several parallel arrays of particles. Consequently, the results given below are based on 31 arrays which contained 31 * 16384 = 507904 particles. Their fate was determined by a single parallel array of random integers (ranging from -32767 to +32767) that was rotated at each temporal step relative to the fixed arrays of particle data, and updated every 31 steps. To implement changes in the pitch-angle cosine, 7 positive integers were chosen in such a way that the probabilities of the current random numbers being larger than this integer are those given by Figure 1. Then the angular index was incremented for those particles whose current random integer was positive and greater than the appropriate probability integer, and decremented for those whose random integer was negative and less than the probability integer with its sign reversed. This approach satisfies the basic requirement that the probabilities of incrementing, decrementing and leaving unchanged the pitch-angle must add to unity. After the pitch-angles had been updated, each particle's distance was changed accordingly. When the desired number of temporal steps had been carried out, particles were binned into an array according to distance and pitch-angle.

ISOTROPIC INJECTION

Results obtained from the MPP for isotropic injection of particles uniformly distributed over pitch-angles are presented in Figure 2 as plots versus distance of the total number of particles in each of 50 bins. This sum over pitch-angles is a measure of the isotropic particle density. Because the total number of particles was large, statistical errors are small and, consequently, are not shown explicitly. However, slight irregularities in some parts of the curves given an indication of their magnitude.

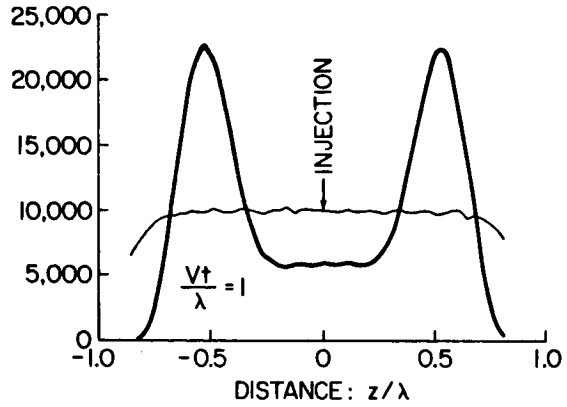

Figure 2. Density profiles shortly after an isotropic injection. The profile for isotropic scattering is featureless, while that for anisotropic scattering exhibits two prominent coherent pulses.

In Figure 2, the darker curve refers to anisotropic scattering (square symbols in Fig. 1), while the lighter one refers to classical isotropic scattering (circular symbols). These density profiles describe a situation very shortly after injection when the particles have had time to move a maximum distance of only one mean free path. The former curve exhibits two peaks, which are completey absent from the latter one. Qualitatively, this manifestation of the coherent mode appears because equal numbers of particles become nearly uniformly distributed in each hemisphere, while very few particles penetrate from one hemisphere to the other through the region of weak scattering near $\mu = 0$. Particles that stay together in each hemisphere, move with nearly the same velocity parallel to the field, but statistical fluctuations of individual velocities give rise to a peak centered around the average displacement. Such features are designated as coherent

pulses. There are two of them in Figure 2 because the injection was symmetrical.

THE COHERENT MODE

A detailed analysis (Ref. 3) predicts that the coherent pulses discussed above form a moving Gaussian density profile given by

$$F = \frac{N_o \exp\left\{-\frac{(z-V_* t)^2}{4\pi D_* t}\right\}}{(4\pi D_* t)^{1/2}}, \qquad (4)$$

where V_* is a characteristic velocity, which is close to half the particle velocity, and D_* is the coefficient of dispersion, which describes the broadening that arises from statistical fluctuations of individual velocities.

Although the isotropic injection of Figure 2 is the most natural choice of initial conditions, it obscures certain important aspects of the coherent mode.

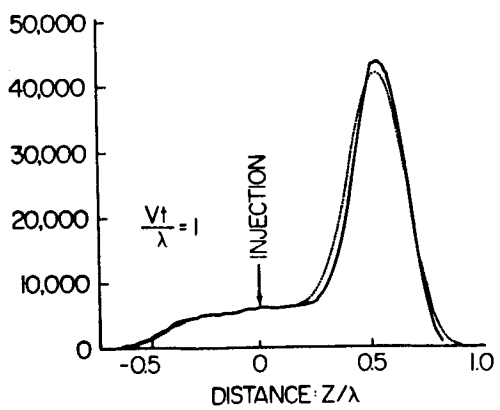

Figure 3. Density profile after a collimated injection, with all other conditions the same as in Figure 2. Evidently, profiles depend sensitively upon conditions at injection. The dotted curve, derived from a finite-difference calculation, is in good, but not perfect agreement with the Monte Carlo results.

Consequently, to bring out these aspects more clearly, this section will focus on highly collimated injection into a region of anisotropic scattering. More specifically, it will deal with injection of particles in the forward hemisphere at a single value $\mu = 0.6$. Figure 3 shows a density profile obtained under these circumstances, but with all other conditions the same as in Figure 2. Evidently, the profile is very sensitive to initial conditions, for only one coherent pulse appears, and, in place of the second pulse, it is accompanied by a broad feature that is designated as the diffusive wake.

The dotted curve gives the result of a finite-difference computation based on Equation 3. The overall agreement is excellent, but there is a slight displacement of the coherent peaks, and the dotted peak is slightly broader than the solid one. The first of these discrepancies is a trivial artifact arising from imperfections in the binning, but the second arises from an important difference between the two computations. More specifically, the finite-difference implementation leads to a dispersive effect which can be described by

$$D_{\#} = \frac{1}{4}V(\Delta z - \frac{1}{2}\Delta s), \qquad (5)$$

and the total dispersion is a superposition of the physical effect described by D_* and the numerical artifact described by $D_{\#}$. In the present example, the condition that ensures that physics dominates, $D_* > D_{\#}$, is met, for $D_* = 4D_{\#}$, but the numerical dispersion is large enough to account for the slight discrepancy between the peaks in Figure 3. To confirm this interpretation, a finite-difference calculation was performed with $D_* = D_{\#}$, and the expected further broadening of the coherent pulse was seen. These details are significant, for they illustrate that the Monte

Carlo method, by virtue of the difference mentioned above in the evolution of z, is relatively free of the artifacts which plague finite-difference calculations. (See Ref. 6 for a discussion of published work that has been affected by such problems.) Numerical dispersion is an especially insidious artifact, for it leads to results that seem plausible, but are quantitatively in error.

ANGULAR DISTRIBUTIONS

To bring out additional features of the coherent mode, Figure 4 shows further results from the anisotropic injection that was discussed above. Here, particle density has been averaged separately over the forward and backward hemispheres. A comparison of the two curves reveals that particles in the pulse are overwhelmingly collimated in the forward direction while those in the wake are predominantly collimated backward. This behavior suggests that the wake can be interpreted as particles scattered out of the pulse which subsequently move coherently away from it in the backward direction.

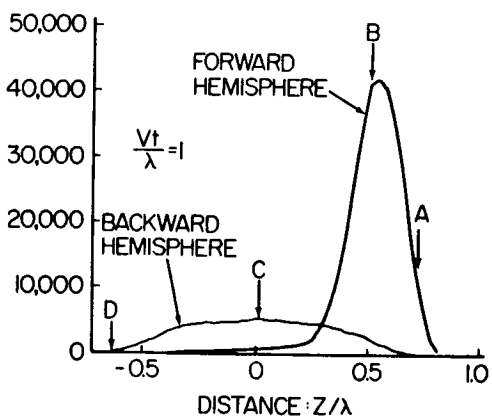

Figure 4. Densities in the forward and backward hemispheres under the same conditions as in Figure 3. The coherent pulse contains particles moving forward. It is accompanied by a broad wake of particles moving backward.

Detailed angular distributions tabulated at four points indicated on Figure 4, and normalized to the same total number of particles, are presented in Figure 5. The distribution at the peak of the pulse (Curve B, circular points) is essentially a mirror image of the one at the center of the wake (Curve C, square points). Both describe near isotropy in one hemisphere associated with nearly zero intensity in the other. This distribution, which is characteristic of the coherent mode, adds weight to the interpretation outlined above.

On the fringes of the density profile, at points A and D, angular distributions (triangular points) are highly collimated in the forward and backward directions, respectively. In the interplanetary context, the fringes would correspond to the the very first particles to arrive in a solar event, which are particularly difficult to describe theoretically, but which are very important in connection with accurate timing of events on the sun. On the MPP, Monte Carlo methods, can give a useful description of this phase of solar events, but statistical fluctuations limit the applicability of the method on less powerful computers.

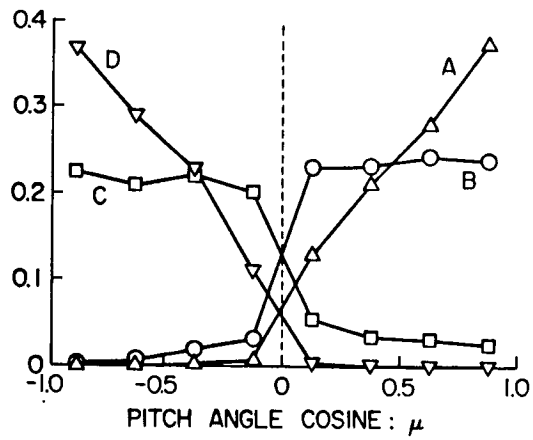

Figure 5. Normalized angular distributions at locations indicated in Figure 4. These distributions exhibit a remarkable mirror symmetry.

THE DIFFUSION LIMIT

Eventually, scattering destroys the strong anisotropies of the coherent mode, and the featureless wake becomes dominant. In this regime, where the familiar theory of diffusion is applicable, the density profile is described by a Gaussian whose width is controlled by the coefficient of diffusion $D = \lambda V/3$ (Ref. 7). Figure 6 shows a profile computed by the MPP in this regime for $Vt = 64 * \lambda$ (solid curve). Evidently, this profile is in very good agreement with the dotted curve which is based upon diffusion theory.

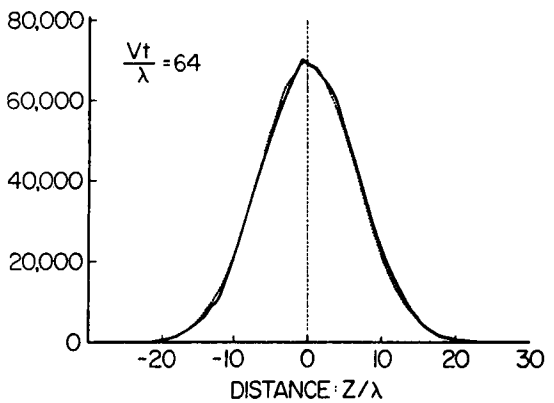

Figure 6. Density profiles in the diffusion regime. Monte Carlo results are in very good agreement with the dotted Gaussian derived from diffusion theory.

CONCLUSIONS

Results obtained from the MPP with the aid of Monte Carlo methods are equivalent in every detail to those based upon careful use of more traditional methods, but they are less subject to error and are closer to the physics. These characteristics offer tremendous advantages in the investigation of exotic transport regimes for which no theoretical description is available. In particular, the formulation of problems in which particles gain or lose energy leads to prohibitively large conventional computations, but their Monte Carlo versions are not significantly more complicated than the one described here. We intend to exploit these advantages in the investigation of two such problems: Adiabatic deceleration of cosmic-rays due to expansion of the solar-wind, and the loss of energy by electrons in radio sources due to synchrotron radiation.

ACKNOWLEDGEMENTS

This research was supported by NASA under Grant NGR-21-002-066.

REFERENCES

1. Lin, R.P., "Emission and Propagation of ~40 keV Solar Flare Electrons", Solar Physics, 15, 453, 1970.

2. Case, K.M. and Zweifel, P.F., "Linear Transport Theory", Addison-Wesley, Reading, MA, 1967.

3. Earl, J.A., "Coherent Propagation of Charged Particle Bunches in Random Magnetic Fields", Astrophysical Journal, 188, 379, 1974.

4. Earl, J.A., "Analytical Description of Charged Particle Transport Along Arbitrary Guiding Field Configurations", Astrophysical Journal, 251, 739, 1981.

5. Jokipii, J.R., "Cosmic-Ray Propagation I, Charged Particles in a Random Magnetic Field", Astrophysical Journal, 146, 480, 1966.

6. Kota, J., Merenyi, E., Jokipii, J.R., Gombosi, T.I. and Owens, A.J., "A Numerical Study of the Pitch-Angle Scattering of Cosmic-Rays", Astrophysical Journal, 254, 398, 1982.

7. Earl, J.A., "The Diffusive Idealization of Charged Particle Transport in Random Magnetic Fields", Astrophysical Journal, 193, 231, 1974.